Crystal Plane Dependent Growth of Aligned Single-Walled Carbon Nanotubes on Sapphire

ARTICLE *in* JOURNAL OF THE AMERICAN CHEMICAL SOCIETY · AUGUST 2008

Impact Factor: 12.11 · DOI: 10.1021/ja8024752 · Source: PubMed

6 AUTHORS, INCLUDING:

Hiroki Ago
Kyushu University
136 PUBLICATIONS **4,476** CITATIONS
SEE PROFILE

Masaharu Tsuji
Kyushu University
440 PUBLICATIONS **6,218** CITATIONS
SEE PROFILE

Konstantin Iakoubovskii
National Institute for Materials Science
81 PUBLICATIONS **1,389** CITATIONS
SEE PROFILE

J|A|C|S
ARTICLES

Published on Web 07/03/2008

Crystal Plane Dependent Growth of Aligned Single-Walled Carbon Nanotubes on Sapphire

Naoki Ishigami,[†] Hiroki Ago,*[,†,‡,§] Kenta Imamoto,[†] Masaharu Tsuji,[†,‡] Konstantin Iakoubovskii,[||] and Nobutsugu Minami[||]

Graduate School of Engineering Sciences, Institute for Materials Chemistry and Engineering, Kyushu University, Kasuga, Fukuoka 816−8580, Japan, PRESTO, Japan Science and Technology Agency (JST), Kawaguchi, Saitama 332-0012, Japan, and Nanotechnology Research Institute, National Institute of Advanced Industrial Science and Technology (AIST), Tsukuba, Ibaraki 305-8565, Japan

Received April 7, 2008; Revised Manuscript Received May 28, 2008; E-mail: ago@cm.kyushu-u.ac.jp

Abstract: On single-crystal substrates, such as sapphire (α-Al_2O_3) and quartz (SiO_2), single-walled carbon nanotubes (SWNTs) align along specific crystallographic axes of the crystal, indicating that the SWNT growth is influenced by the crystal surface. Here, we show that not only the orientation, but also the diameter and chirality of SWNTs are affected by the crystal plane of the sapphire substrate. The aligned SWNTs grown on the A- and R-planes of sapphire have narrower diameter distributions than randomly oriented tubes produced on the C-plane sapphire and amorphous SiO_2. Photoluminescence measurements reveal a striking difference between the aligned SWNTs: near-zigzag tubes are observed on the A-plane and near-armchair tubes on the R-plane. This study shows the route for the diameter and chirality control of SWNTs by surface atomic arrangements of a single-crystal substrate.

Introduction

Single-walled carbon nanotubes (SWNTs) are a promising material for nanoelectronics because of their excellent electronic and physical properties.[1] It is essential to control the position, orientation, and electronic structure of a large number of SWNTs attached to a substrate in order to realize nanotube-based devices, such as field-effect transistors (FETs),[2] logic circuits,[3] and sensors.[4] There are two major approaches for the fabrication of these devices: one is to utilize postsynthesis separation together with patterning techniques, and the other is to synthesize nanotubes directly on a substrate in a highly controlled manner. Although the metal-semiconductor separation has recently been demonstrated,[5,6] drawbacks of the postsynthesis separation are sonication-induced damage and contamination during the dispersion process, which result in shortened nanotubes ($<1\ \mu$m) and deteriorated transport properties.

The growth of SWNTs directly on a substrate, on the other hand, can produce long SWNTs with clean surfaces. The position of SWNTs is usually defined by the catalyst patterning achieved with conventional lithography,[7,8] ink-jet printing,[9] or microcontact printing[10] techniques. One can control the SWNT growth direction by, e.g., electric field,[11] gas-flow,[12] or self-organized alignment utilizing the atomic steps[13−15] or orientation[15−20] of single-crystal substrate surfaces. The self-organized alignment method produces dense and highly aligned SWNT networks without any special technique or equipment.

However, the selective growth of semiconducting SWNTs or SWNTs with a unique chirality is still challenging. Recent studies demonstrated the synthesis of SWNTs with narrow chirality distributions through the optimization of growth conditions, such as temperature,[21−23] catalyst metal,[21,24] catalyst support,[23] pres-

[†] Graduate School of Engineering Sciences, Kyushu University.
[‡] Institute for Materials Chemistry and Engineering, Kyushu University.
[§] PRESTO-JST.
[||] Nanotechnology Research Institute, AIST.

(1) Saito, R.; Dresselhaus, G.; Dresselhaus, M. S. *Physical Properties of Carbon Nanotubes*; Imperial College Press: London,1998.
(2) Tans, S. J.; Verschueren, A. R. M.; Dekker, C. *Nature* **1998**, *393*, 49.
(3) Chen, Z.; Appenzeller, J.; Lin, Y. M.; Sippel-Oakley, J.; Rinzler, A. G.; Tang, J.; Wind, S. J.; Solomon, P. M.; Avouris, P. *Science* **2006**, *311*, 1735.
(4) Kong, J.; Franklin, N. R.; Zhou, C.; Chapline, M. G.; Peng, S.; Cho, K.; Dai, H. *Science* **2000**, *287*, 622.
(5) Strano, M. S.; Dyke, C. A.; Usrey, M. L.; Barone, P. W.; Allen, M. J.; Shan, H.; Kittrell, C.; Hauge, R. H.; Tour, J. M.; Smalley, R. E. *Science* **2003**, *301*, 1519.
(6) Arnold, M. S.; Green, A. A.; Hulvat, J. F.; Stupp, S. I.; Hersam, M. C. *Nat. Nanotech.* **2006**, *1*, 60.
(7) Ishida, M.; Hongo, H.; Nihey, F.; Ochiai, Y. *Jpn. J. Appl. Phys., Part 2* **2004**, *43*, L1356.
(8) Javey, A.; Dai, H. *J. Am. Chem. Soc.* **2005**, *127*, 11942.
(9) Ago, H.; Murata, K.; Yumura, M.; Yotani, J.; Uemura, S. *Appl. Phys. Lett.* **2003**, *82*, 811.
(10) Gu, G.; Philipp, G.; Wu, X.; Burghard, M.; Bittner, A. M.; Roth, S. *Adv. Funct. Mater.* **2001**, *11*, 295.
(11) Ural, A.; Li, Y.; Dai, H. *Appl. Phys. Lett.* **2002**, *81*, 3464.
(12) Huang, S.; Cai, X.; Du, C.; Liu, J. *J. Phys. Chem. B* **2003**, *107*, 13251.
(13) Ismach, A.; Segev, L.; Wachtel, E.; Joselevich, E. *Angew. Chem., Int. Ed.* **2004**, *43*, 6140.
(14) Kocabas, C.; Hur, S. H.; Gaur, A.; Meitl, M. A.; Shim, M.; Rogers, J. A. *Small* **2005**, *1*, 1110.
(15) Ago, H.; Imamoto, K.; Ishigami, N.; Ohdo, R.; Ikeda, K.; Tsuji, M. *Appl. Phys. Lett.* **2007**, *90*, 123112.
(16) Ago, H.; Nakamura, K.; Ikeda, K.; Uehara, N.; Ishigami, N.; Tsuji, M. *Chem. Phys. Lett.* **2005**, *408*, 433.
(17) Ago, H.; Uehara, N.; Ikeda, K.; Ohdo, R.; Nakamura, K.; Tsuji, M. *Chem. Phys. Lett.* **2006**, *421*, 399.
(18) Han, S.; Liu, X.; Zhou, C. *J. Am. Chem. Soc.* **2005**, *127*, 5294.
(19) Kocabas, C.; Kang, S. J.; Ozel, T.; Shim, M.; Rogers, J. A. *J. Phys. Chem. C* **2007**, *111*, 17879.
(20) Ding, L.; Yuan, D.; Liu, J. *J. Am. Chem. Soc.* **2008**, *130*, 5428.
(21) Miyauchi, Y.; Chiashi, S.; Murakami, Y.; Hayashida, Y.; Maruyama, S. *Chem. Phys. Lett.* **2004**, *387*, 198.

10.1021/ja8024752 CCC: $40.75

sure,[25] and carbon precursor.[23,26] Nevertheless, neither perfect control of chirality nor selective growth of semiconducting SWNTs has been achieved so far. Selective plasma etching of metallic SWNTs was reported,[27,28] but it deteriorates the transport properties of semiconducting SWNTs, probably due to side reactions.

Several theoretical and experimental studies have suggested that nanotube chirality depends on the cap structure, like a hemisphere of fullerenes, formed on a metal nanoparticle catalyst in the early stage of SWNT growth.[29–31] Therefore, it should be important to control the structure of metal catalysts for the selective growth of SWNTs with specific chiralities. One possible approach to this selective SWNT growth is to utilize the epitaxial interaction between the metal catalyst and a single-crystal substrate. The direct interaction between the cap of a nanotube and the crystal surface is another possibility. Single-crystal sapphire (α-Al_2O_3) is widely used for the epitaxial growth of compound semiconductor films, such as AlGaN, GaN, and ZnO, which are applied to light-emitting diodes and lasers.[32] In addition, Fe−Mo and Co metals are also reported to form epitaxial films on a sapphire suface.[33–35] Therefore, influence of the sapphire surface on nanotube structure is interesting from the viewpoint of epitaxial growth.

Hongo et al. reported that the yield of SWNT growth on sapphire depends on the crystal orientation, thus suggesting a route of controlling the nanotube growth.[36] More recently, we demonstrated horizontally aligned growth of SWNTs along specific crystallographic axes on the A-plane ($11\bar{2}0$) and R-plane ($1\bar{1}02$) sapphire but not on the C-plane (0001).[16,17] Because the growth direction is predetermined by a crystallographic direction on the A- and R-planes, we called this process an "atomic arrangement programmed growth". Polarized Raman measurements confirmed the aligned growth of SWNTs,[17] but the detailed characterization of the SWNTs has not been performed so far, except for the analysis of transport properties.[37]

Photoluminescence (PL) and resonance Raman spectroscopies are powerful tools for the assignment of the chiral index (n, m) of SWNTs. However, PL measurements from as-grown SWNTs lying on a substrate were rather difficult, because interaction with the substrate quenches the PL from SWNTs.[38,39] In this study, we investigated the diameters and chiralities of as-grown SWNTs on different planes of sapphire using Raman and PL spectroscopies. The SWNTs aligned on the A-plane showed narrow chirality distribution and near-zigzag structure with small chiral angles, whereas the SWNTs on the R-plane showed relatively wide chirality distributions with dominant emission from near-armchair tubes (chiral angle ~30°). These results suggest the possibility of chirality-selective growth based on the interaction between the metal catalyst (or the SWNT) and the crystal surface.

Experimental Section

Sapphire substrates with a misorientation <0.3° (KYOCERA Corp., Japan) were cleaned by sonication in acetone and isopropyl alcohol. An Si (1 0 0) substrate with a thermally grown SiO_2 layer (thickness, 300 nm) was also used for comparison. Although we have applied Fe-based catalysts for the SWNT growth in our previous studies,[15–17] a Co−Mo-based catalyst was utilized here, because it supported SWNT growth in the wider temperature range (750−900 °C). The Co−Mo catalyst was dip-coated by introducing a substrate into the ethyl alcohol solution of cobalt (II) nitrate hexahydrate ($Co(NO_3)_2 \cdot 6H_2O$) and bis(acetylacetonate)dioxomolybdenum ($MoO_2(acac)_2$) with an atomic ratio of Co:Mo = 94:6 and then dried in air. For chemical vapor deposition (CVD) growth of SWNTs, a substrate was loaded into a quartz tube of an electric furnace and heated in a flow of 300 sccm Ar under atmospheric pressure. After reaching the CVD temperature (750−900 °C), the catalyst was reduced in an H_2 gas flow for 10 min and then reacted with a CH_4/H_2 gas mixture (H_2 7 vol%) flowing at a rate of 1000 sccm.

The structures of the as-grown SWNTs and catalysts were studied with atomic force microscopy (AFM, Veeco Nanoscope IIIa) and scanning electron microscopy (SEM, HITACHI S-4800). Resonant micro-Raman spectra were obtained using a JASCO NRS-2100 spectrometer equipped with Ar ion (488, 514 nm) and He−Ne lasers (633 nm). We used the VV configuration to effectively measure the aligned SWNTs, where the incident and scattered beams were polarized parallel to them. PL spectra were measured with a setup[40] utilizing a continuous-wave Ti-sapphire laser (700−1030 nm) and a liquid nitrogen-cooled InGaAs detector (900−1650 nm). The laser power and spot size were approximately 1 W and 1 mm, respectively. The chiralities were assigned using the data reported by Weisman and Bachilo.[41]

Results and Discussion

AFM Characterization of the Catalyst. The substrates for SWNT growth were dip-coated by Co−Mo salts. Elevating the temperature in Ar followed by reduction in H_2 decomposed the salts into metal nanoparticles which acted as the catalyst of the subsequent SWNT growth. The particle diameter is essential for growth, and it was separately evaluated by AFM for the samples reduced at 900 °C in a H_2 flow. The AFM images and histograms of the nanoparticle height are depicted in Figure 1. The mean diameter of nanoparticles was strongly dependent on the crystal plane, and it increased in the order of A-plane (0.6 ± 0.5 nm) < R-plane (1.6 ± 0.7 nm) < SiO_2 (1.7 ± 0.6 nm) < C-plane (4.8 ± 4.0 nm). We would note that the absolute AFM values could be affected by the process-induced substrate inhomogeneities, and the relative AFM trends are more reliable. Those substrate inhomogeneities should, however, be much weaker in the catalyst assessment than in the SWNT pictures

(22) Ago, H.; Imamura, S.; Okazaki, T.; Saito, T.; Yumura, M.; Tsuji, M. *J. Phys. Chem. B* **2005**, *109*, 10035.
(23) Lolli, G.; Zhang, L.; Balzano, L.; Sakulchaicharoen, N.; Tan, Y.; Resasco, D. E. *J. Phys. Chem. B* **2006**, *110*, 2108.
(24) Bachilo, S. M.; Balzano, L.; Herrera, J. E.; Pompeo, F.; Resasco, D. E.; Weisman, R. B. *J. Am. Chem. Soc.* **2003**, *125*, 11186.
(25) Wang, B.; Wei, L.; Yao, L.; Li, L.; Yang, Y.; Chen, Y. *J. Phys. Chem. C* **2007**, *111*, 14612.
(26) Wang, B.; Poa, C. H. P.; Wei, L.; Li, L.; Yang, Y.; Chen, Y. *J. Am. Chem. Soc.* **2007**, *129*, 9014.
(27) Zhang, G.; Qi, P.; Wang, X.; Lu, Y.; Li, X.; Tu, R.; Bangsaruntip, S.; Mann, D.; Zhang, L.; Dai, H. *Science* **2006**, *314*, 974.
(28) Ohnaka, H.; Kojima, Y.; Kishimoto, S.; Ohno, Y.; Mizutani, T. *Jpn. J. Appl. Phys.* **2006**, *45*, 5485.
(29) Reich, S.; Li, L.; Robertson, J. *Phys. Rev. B* **2005**, *72*, 165423.
(30) Ding, F.; Larsson, P.; Larsson, J. A.; Ahuja, R.; Duan, H.; Rosén, A.; Bolton, K. *Nano Lett.* **2008**, *8*, 463.
(31) Hofmann, S. *Nano Lett.* **2007**, *7*, 602.
(32) *Atomistic Aspects of Epitaxial Growth*; Kotrla, M., Papanicolaou, N. I., Vvedensky, D. D., Wille, L. T., Eds.; Kluwer Academic Publishers: Nederlands, 2002.
(33) Fraune, M.; Hauch, J. O.; Güntherodt, G.; Laufenberg, M.; Fonin, M.; Rüdiger, U.; Mayer, J.; Turban, P. *J. Appl. Phys.* **2006**, *99*, 033904.
(34) Shi, H. T.; Lederman, D. *Phys. Rev. B* **1998**, *58*, R1778.
(35) Espinosa, J.; Shi, H.; Lederman, D. *J. Appl. Phys.* **2006**, *99*, 023516.
(36) Hongo, H.; Yudasaka, M.; Ichihashi, T.; Nihey, F.; Iijima, S. *Chem. Phys. Lett.* **2002**, *361*, 349.
(37) Ago, H.; Ishigami, N.; Imamoto, K.; Suzuki, T.; Ikeda, K. Tsuji, M.; Ikuta, T.; Takahashi, K. *J. Nanosci. Nanotech.*, in press.
(38) Xie, L.; Liu, C.; Zhang, J.; Zhang, Y.; Jiao, L.; Jiang, L.; Dai, L.; Liu, Z. *J. Am. Chem. Soc.* **2007**, *129*, 12382.
(39) Lefebvre, J.; Finnie, P. *Phys. Rev. Lett.* **2007**, *98*, 167406.
(40) Iakoubovskii, K.; Minami, N.; Kazaoui, S.; Ueno, T.; Miyata, Y.; Yanagi, K.; Kataura, H.; Ohshima, S.; Saito, T. *J. Phys. Chem. B* **2006**, *110*, 17420.
(41) Weisman, R. B.; Bachilo, S. M. *Nano Lett.* **2003**, *3*, 1235.

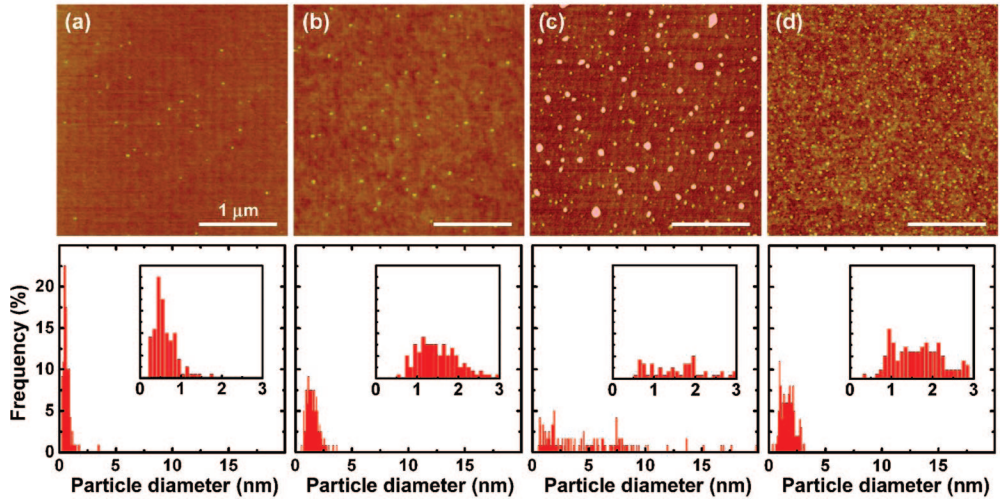

Figure 1. AFM images and diameter distributions of metal nanoparticles on (a) A-, (b) R-, and (c) C-plane sapphire substrates and on (d) oxidized silicon substrates. These images were obtained after the reduction of the Co−Mo metal salt with H_2 at 900 °C for 10 min. The total number of counted metal nanoparticles is 120.

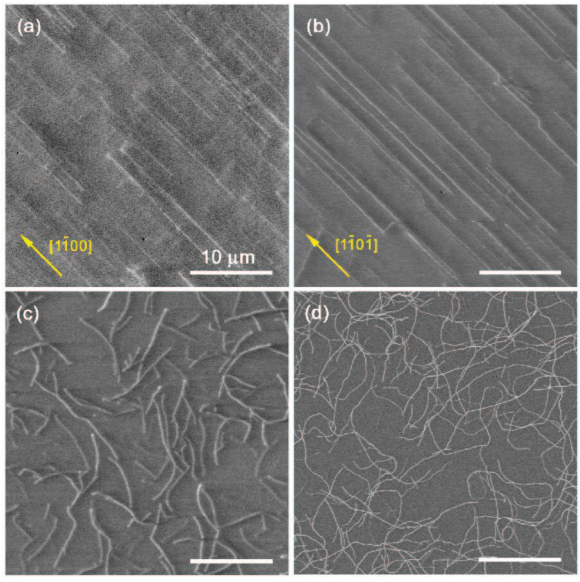

Figure 2. SEM images of SWNTs grown at 900 °C on (a) A-, (b) R-, and (c) C-plane sapphire substrates, and on (d) oxidized silicon substrate.

because of the shorter and cleaner (H_2 only, i.e., no CH_4 decomposition) gas environment.

Regarding the observed diameter differences, we would note that the surface energies of the A-, R-, and C-planes were calculated as 2.39, 2.14, and 1.85 J/m^2, respectively.[42] Although the surface state of a sapphire substrate might be changed by the heat treatment, this trend explains well the difference in the diameter distribution of the metal nanoparticles of Figure 1. The particles adhere better to the A- and R-sapphire planes having higher surface energies and thus do not aggregate much, while the aggregation is enhanced on the C-plane due to its lower surface energies.

SEM Observations of the Nanotubes. The substrates covered with Co−Mo metal nanoparticles were then used for the SWNT synthesis. Figure 2 shows SEM images of SWNTs grown over a Co−Mo binary catalyst supported on A-, R-, and C-plane sapphire and oxidized silicon substrates at 900 °C. Note that the substrates are electrically insulating, and thus the SWNTs appeared thick due to the electron beam-induced charging. As we reported previously, SWNTs are aligned along the specific crystallographic axes on the A- and R-planes.[16,17] This alignment represents the anisotropic van der Waals interaction between SWNTs and the sapphire substrate. Alternatively, SWNTs grew randomly on the C-plane, as is the case of oxidized silicon substrates. The random orientation of SWNTs is accounted for by the isotropic interaction with the oxidized silicon or the high-symmetry C-plane of sapphire.

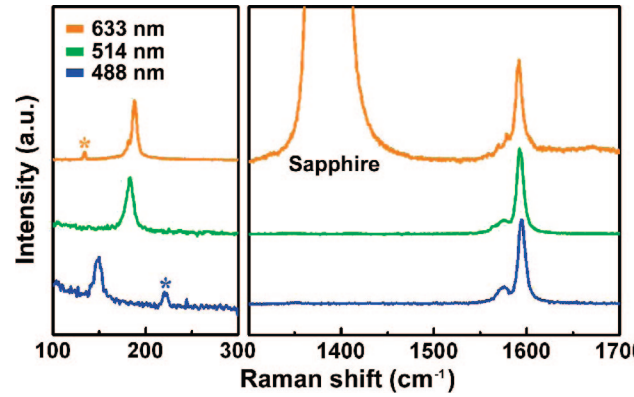

Figure 3. Raman spectra of aligned SWNTs grown at 900 °C on A-plane sapphire measured with three excitation wavelengths (488, 514, and 633 nm). The asterisks indicate the peaks originating from the excitation light.

Raman Scattering Results. The Raman spectra of SWNTs grown on the four different substrates were measured with three different excitation wavelengths (488, 514, and 633 nm). Figure 3 presents the typical Raman spectra measured for the aligned SWNTs on A-plane sapphire. They show a clear G-band at ~1592 cm^{-1}, almost negligible defect-induced D-band at ~1350 cm^{-1}, and low-frequency radial breathing modes (RBMs). The intensity ratio of the former two bands (I_G/I_D) was greater than 110 indicating the high SWNT quality. Because the sapphire substrates give peaks only in the range of 300−1500 cm^{-1}, we could easily distinguish the RBM peaks from others and estimate, from the RBM position, the SWNT diameter. In the case of single-crystal quartz, two strong peaks originating in

(42) Sun, J.; Stirner, T.; Matthews, A. *Surf. Coat. Technol.* **2006**, *201*, 4205.

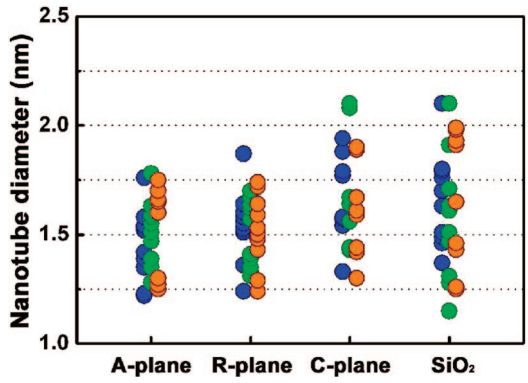

Figure 4. Diameters of SWNTs deduced from the Raman spectra. Blue, green, and orange circles represent the data measured with 488, 514, and 632 nm excitations, respectively.

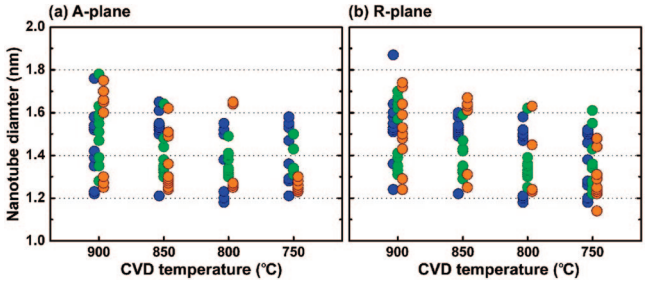

Figure 5. Diameters of SWNTs deduced from the Raman spectra as a function of the CVD growth temperature on the A-plane (a) and R-plane (b) sapphire substrates. The symbol colors are the same as in Figure 4.

the substrate appear at low wavenumbers (100−250 cm^{-1}).[19] They overlap with the RBM signals, making difficult to assess the SWNT diameters.

Using the RBM signals, we have estimated the SWNT diameters on A-, R-, C-plane sapphire and oxidized silicon substrates as follows: each substrate was widely scanned by moving the sample stage automatically and measuring the Raman spectra. For each excitation wavelength, 10 different RBM spectra were collected (Figure 4). The nanotube diameter d_{NT} (nm) was calculated as $d_{NT} = 248/\omega_{RBM}$, where ω_{RBM} is the RBM frequency (cm^{-1}). We did not use the AFM height profiles to analyze the SWNT diameter distributions, because the AFM diameters were affected by the substrate (see Supporting Information, S-1). Interestingly, we found that the aligned SWNTs on the A- and R-plane sapphire surfaces have smaller diameters (1.2−1.8 nm) than the SWNTs randomly oriented on the C-plane (1.3−2.2 nm). This tendency is consistent with the observed diameters of the Co−Mo metal nanoparticles (see Figure 1). These results signify that not only the growth direction but also the nanotube diameter is influenced by the crystal surface.

The SWNT diameter is mainly determined by three factors: catalyst particle size, hydrocarbon feedstock, and CVD temperature. The hydrocarbon feedstock and CVD temperature were the same for all of the substrates. Therefore, we speculate that the narrow diameter variations of SWNTs on R- and A-planes is realized by an indirect effect of the crystal orientation, through altering the size of the catalyst nanoparticles.

The temperature dependences of SWNT diameters for the A- and R-plane sapphire substrates are plotted in Figure 5. On both of the substrates, the diameter variations of SWNTs became narrower with decrease in the CVD temperature. In particular, the formation of large-diameter nanotubes was suppressed at low temperatures. This can be explained by the suppression of the thermal agglomeration of the metal nanoparticle catalyst at lower temperatures.[21,22]

It is important to note that the data of Figures 4 and 5 merely show relative trends in the nanotube diameters as a function of the growth plane and temperature. Because of insufficient statistics and difficulties in normalizing Raman intensity, those data only indicate presence of certain nanotubes, but not their abundance. Besides, the Raman excitation selectively probed those nanotubes whose bandgap was in resonance with the laser, but whose relative density could be small. Much more reliable data on the nanotube diameter were obtained with the PL as discussed below.

Photoluminescence Results. The near-infrared PL spectroscopy is a powerful tool for characterizing the chiralities of semiconducting SWNTs. However, the PL from SWNTs is strongly quenched when the SWNTs are directly deposited on a substrate.[38,39] The detailed mechanism of this PL quenching is still unclear, but it is explained by the formation of nonradiative recombination centers at the SWNT-substrate interface. Xie et al. suggested that the formation of C−O covalent bonds between an SWNT and a SiO_2 surface in a CVD process creates new energy levels in the energy gap of a semiconducting SWNT.[38] Nevertheless, we have succeeded in measuring PL contour maps from SWNTs on sapphire, as shown in Figure 6. To the best of our knowledge, this is the first observation of PL from as-grown SWNTs lying on a substrate. Several reasons could account for this successful observation: (1) enhanced sensitivity of our PL setup, (2) growth of high-density arrays of isolated SWNTs, (3) partial detachment of SWNTs from the substrate, and (4) negligible PL background from the sapphire substrates. On the contrary, strong signals from a Si substrate hindered PL measurements of SWNTs on oxidized silicon.

Note that traditional preparation of PL samples involves SWNT dispersion and centrifugation, which do alter the SWNT diameter distribution. The PL measurements reported here of as-grown samples can provide more reliable information on the SWNT diameters and chirality. This information is, however, affected by the chirality dependence of PL quantum yield which has been neglected here.

The contour maps of many as-grown SWNT samples (Figure 6) exhibit broad features with partially resolved chiralities; the broadening can be attributed to the SWNT-substrate interaction. It could be possible that the measured PL originated from SWNTs, which for some reason have mostly detached from the substrate. Those SWNTs would then lose the substrate-induced alignment that could be detected in polarization-resolved PL measurements.[39] An example of this is shown in Figure 7 for the SWNTs on R-plane sapphire. Strong alignment (polarization ratio ∼15) is observed, revealing that the SWNTs are attached to the substrate. We cannot, however, exclude a possibility that some SWNT segments, in a caterpillar-like fashion, lost intimate contact with the substrate while remaining parallel to the tube axis.

The dependences of PL intensity on SWNT diameter and chiral angle are presented in Figure 8. The chirality distributions are much wider for the R-plane compared to the A-plane of sapphire. It is important to note that the SWNTs with diameters over 1.4 nm could not be detected in these PL measurements. The chirality distributions of SWNTs on the A-plane (Figure

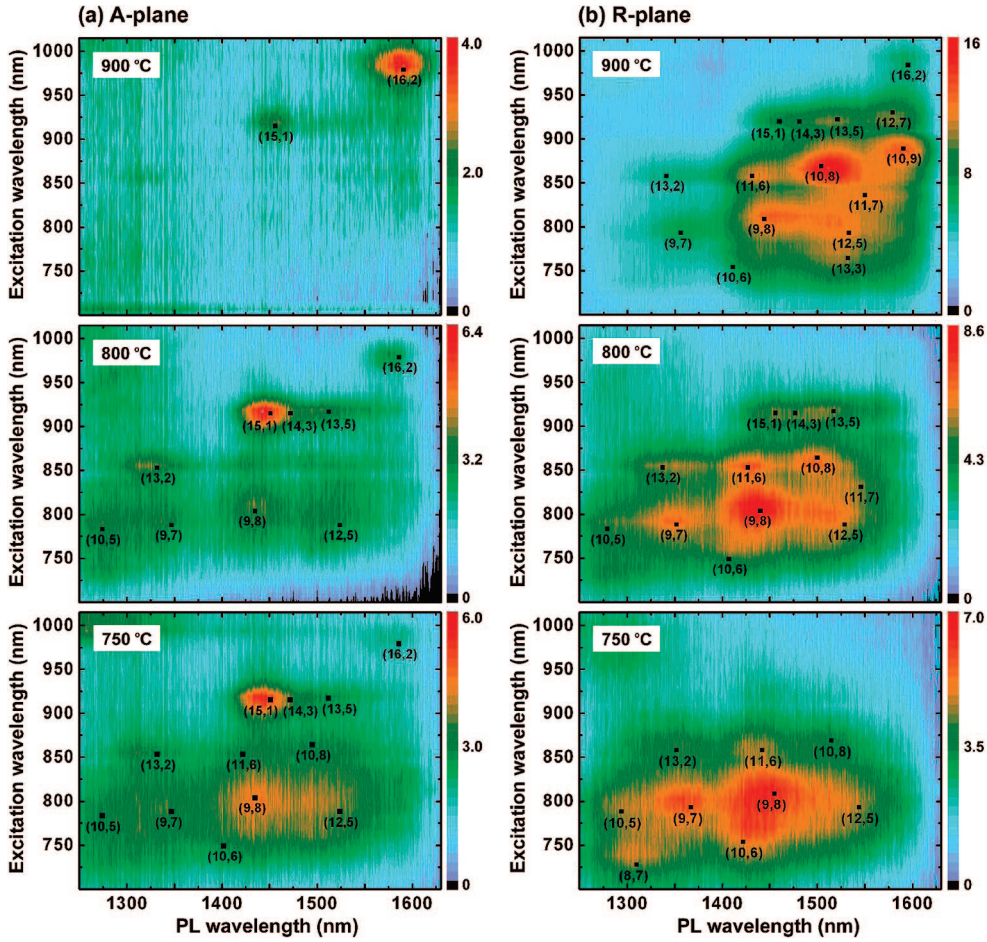

Figure 6. PL contour maps of the as-grown SWNTs on A- and R-plane sapphire at different CVD temperatures.

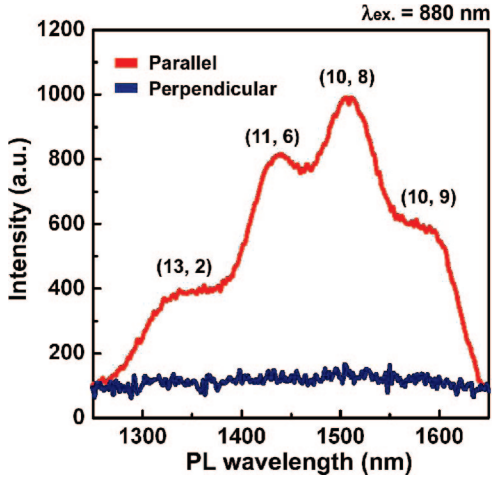

Figure 7. Polarized PL spectra of the aligned SWNTs grown on the R-plane substrate measured with 880 nm excitation. Red and blue lines indicate the PL spectra measured parallel and perpendicular to the orientation of the SWNTs, respectively.

8a) suggest preferential growth of near-zigzag (16, 2) SWNT at 900 °C, (15, 1) tubes at 800 °C, and (15, 1) and (9, 8) tubes at 750 °C. On the contrary, PL from the SWNTs grown on the R-plane (Figure 8b) is dominated by the near-armchair SWNTs for all the CVD temperatures studied.

Vast numbers of reports reveal that near-armchair tubes dominate the PL spectra from SWNTs of different diameters, grown by various techniques such as CVD[21–26,43] and laser ablation.[43,44] The exact population density of each (n, m) SWNT cannot be estimated from the PL intensity, because the fluorescence quantum yield has not been experimentally determined for all of the chiralities shown in Figure 6.[45] However, since the aligned SWNTs on A- and R-planes have the similar diameter distributions (Figure 4 and Supporting Information S-1), the preferential growth of near-zigzag SWNTs on the A-plane is reliable. Note that we cannot assign many chiralities, such as (15, 1) and (16, 2), to the specific RBM peaks of the Raman spectra, because these SWNTs are not resonant with the excitation wavelengths used in this study.[46] Figure 6 reveals that the chirality distribution shifted toward small diameters with lowering CVD temperature on both A- and R-planes. This observation is consistent with the result of the Raman measurements (see Figure 5).

Red Shift of PL Peaks. The ovals in the PL maps of Figure 6 uniquely determine the first and second transition energies, E_{11} and E_{22}, of the SWNTs: excitation of the E_{22} transitions, after internal relaxation, leads to PL emission from the E_{11}

(43) Okazaki, T.; Saito, T.; Matsuura, K.; Ohshima, S.; Yumura, M.; Oyama, Y.; Saito, R.; Iijima, S. *Chem. Phys. Lett.* **2006**, *420*, 286.
(44) Lebedkin, S.; Arnold, K.; Hennrich, F.; Krupke, R.; Renker, B.; Kappes, M. M. *New. J. Phys.* **2003**, *5*, 140.
(45) Tsyboulski, D. A.; Rocha, J. R.; Bachilo, S. M.; Cognet, L.; Weisman, R. B. *Nano Lett.* **2007**, *7*, 3080.
(46) Araujo, P. T.; Doorn, S. K.; Kilina, S.; Tretiak, S.; Einarsson, E.; Maruyama, S.; Chacham, H.; Pimenta, M. A.; Jorio, A. *Phys. Rev. Lett.* **2007**, *98*, 067401.

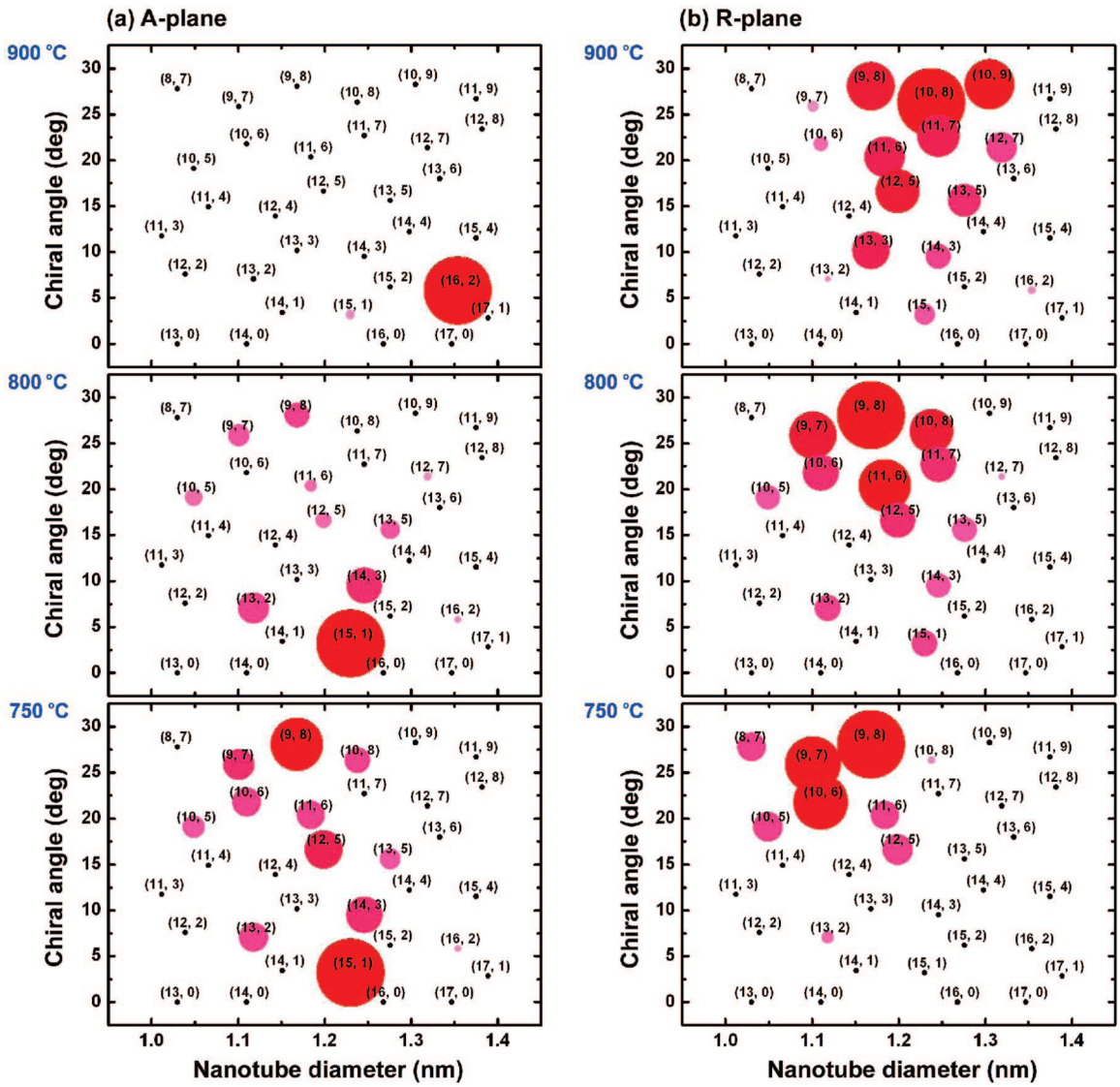

Figure 8. Luminescence intensity and chirality distribution of the SWNTs grown on sapphire surfaces at different CVD temperatures. The diameter of the circle and the color contrast represent the relative PL intensity.

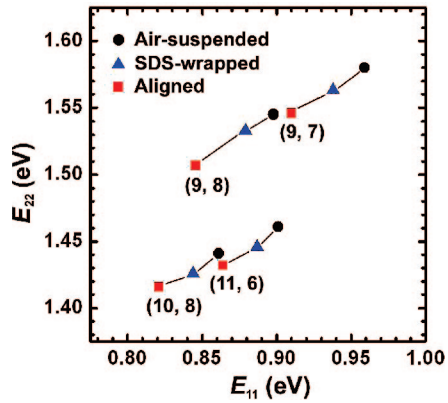

Figure 9. Optical transition energies, E_{11} and E_{22}, of air-suspended,[47] SDS-wrapped,[41] and aligned SWNTs (present work) derived from PL measurements.

transition. The E_{11} and E_{22} values have been extracted from the PL spectra of four SWNTs with different chiralities grown on R-plane sapphire and plotted in Figure 9. The data of the air-suspended SWNTs grown on a trenched quartz substrate by CVD,[47] and those of the sodium dodecyl sulfate (SDS) wrapped SWNTs[41] are also shown for comparison. Not all of the chiralities are plotted in Figure 9 because of the lack of the reference PL data or broadness and weakness of some PL feature in our spectra.

We found that the E_{11} and E_{22} transitions of our aligned SWNTs are red-shifted by ~45 meV for E_{11} and ~32 meV for E_{22} peaks as compared to those of air-suspended SWNTs.[47] It is well-known that both E_{11} and E_{22} values are sensitive to the SWNT environment and can shift to higher or lower energies depending on the bundling,[48] temperature,[48,49] charge transfer,[50] dielectric screening,[47,51–53] and deformation (strain).[54,55] In our study, most of the aligned SWNTs are isolated, and the laser-

(47) Ohno, Y.; Iwasaki, S.; Murakami, Y.; Kishimoto, S.; Maruyama, S.; Mizutani, T. *Phys. Rev. B* **2006**, *73*, 235427.
(48) Fantini, C.; Jorio, A.; Souza, M.; Strano, M. S.; Dresselhaus, M. S.; Pimenta, M. A. *Phys. Rev. Lett.* **2004**, *93*, 147406.
(49) Zhang, Y.; Son, H.; Zhang, J.; Kong, J.; Liu, Z. *J. Phys. Chem. C* **2007**, *111*, 1988.
(50) Shim, M.; Ozel, T.; Gaur, A.; Wang, C. *J. Am. Chem. Soc.* **2006**, *128*, 7522.
(51) Kiowski, O.; Lebedkin, S.; Hennrich, F.; Malik, S.; Rösner, H.; Arnold, K.; Sürgers, C.; Kappes, M. M. *Phys. Rev, B* **2007**, *75*, 075421.

induced heating effect should be small because of the high thermal conductivity and optical transparency of sapphire substrates and strong SWNT-substrate interaction. Analysis of the G-band in our Raman spectrum suggests negligible charge transfer between SWNT and a sapphire substrate: the charge transfer to SWNTs induces the down- or upshift of the G-band,[56] but we did not observe any shift in the G-band for the aligned SWNTs on sapphire. Thus, we suggest that dielectric screening and/or deformation brought the red shift into our PL spectra. As for the dielectric screening, the Coulomb interaction between the electron−hole pairs in SWNTs decreases with increase in the dielectric constant of the environment, thus resulting in the red shift in the PL spectra. It is known that a larger dielectric constant reduces the E_{11} and E_{22} values.[52–54] The dielectric constants of air and water−surfactant environments are 1.0 and ~2, respectively.[51] Considering the higher dielectric constant of sapphire (3.1),[57] we suggest that dielectric screening is the primary reason of the observed red-shift. In addition, the SWNT alignment indicates strong interaction between the sapphire substrate and SWNTs, which may produce strain in the SWNTs and thus also contribute to the observed red shift of the E_{11} and E_{22} energies.

Mechanism of Chirality Dependent Growth. This study demonstrates the chirality-dependent growth of nanotubes on the A- and R-plane sapphire, and in this section, we would briefly comment on the possible reasons for this selectivity. The nanotube chirality is determined by the cap structure initially formed on the metal nanoparticles.[29–31] In our growth process, those metal nanoparticles are produced from the Co−Mo salts covering the sapphire substrate, through heat- and gas-flow assisted decomposition. It is reasonable to suggest that the dissimilar atomic structures of the A- and R-plane sapphire surfaces induce differences in the particle morphology and orientation thereby affecting the SWNT chirality. Another possible explanation is the formation of specific cap structures during the initial growth due to the direct interaction with the different atomic arrangements of the sapphire surfaces. In other words, the epitaxial relationship due to the matching of the lattice constants of sapphire and a specific SWNT may lead to the crystal plane-dependent growth. The surface atomic structures of the A- and R-plane sapphire with overlaying graphene sheets are illustrated in the Supporting Information (S-2). It is difficult to rationalize the two lattice structures, which may be related with the initial nucleation step of the SWNT growth at high temperature. Further study, such as high-resolution microscopy, is also required to reveal the SWNT growth mechanism.

Conclusions

We have investigated the influence of the surface atomic arrangement of sapphire on the diameter and chirality of horizontally aligned SWNTs using Raman and PL spectroscopies. Raman measurements suggest that aligned SWNTs on the A- and R-planes have narrower diameter distributions compared with randomly oriented SWNTs on the C-plane and oxidized silicon. We have succeeded in measuring the PL spectra from as-grown SWNTs on sapphire. They showed a large red shift in the first and second band gap energies, E_{11} and E_{22}, probably due to the influence of the substrate. The emission from the near-armchair SWNTs was mainly observed on the R-plane substrate, as is the case in micelle-encapsulated SWNTs synthesized by CVD and laser-ablation methods. However, PL from the near-zigzag SWNTs was observed on the A-plane. These results suggest that the atomic arrangements of sapphire affect the diameter and chirality of SWNTs along with their growth direction. We hope that these findings will develop into highly controlled "epitaxial nanotube growth".

Acknowledgment. This work was supported by PRESTO-JST, a Grant-in-Aid for Scientific Research from the MEXT, and the Industrial Technology Research Program from NEDO.

Supporting Information Available: AFM images and height distributions of SWNTs grown on sapphire and SiO_2/Si substrates, surface atomic structures of A- and R-planes sapphire together with a graphene sheet, and complete ref 31. This material is available free of charge via the Internet at http://pubs.acs.org.

JA8024752

(52) Miyauchi, Y.; Saito, R.; Sato, K.; Ohno, Y.; Iwasaki, S.; Mizutani, T.; Jiang, J.; Maruyama, S. *Chem. Phys. Lett.* **2007**, *442*, 394.
(53) Ohno, Y.; Iwasaki, S.; Murakami, Y.; Kishimoto, S.; Maruyama, S.; Mizutani, T. *Phys. Stat. Sol. b* **2007**, *244*, 4002.
(54) Filho, A. G. S.; Kobayashi, N.; Jiang, J.; Grüneis, A.; Saito, R.; Cronin, S. B.; Filho, J. M.; Samsonidze, G. G.; Dresselhaus, G.; Dresselhaus, M. S. *Phys. Rev. Lett.* **2005**, *95*, 217403.
(55) Zhang, Y.; Zhang, J.; Son, H.; Kong, J.; Liu, Z. *J. Am. Chem. Soc.* **2005**, *127*, 17156.
(56) Rao, A. M.; Eklund, P. C.; Bandow, S.; Thess, A.; Smalley, R. E. *Nature* **1997**, *388*, 257.
(57) Schubert, M.; Tiwald, T. E.; Herzinger, C. M. *Phys. Rev. B* **2000**, *61*, 8187.